Imaging the Local Charge Environment of Nitrogen-Vacancy Centers in Diamond

T. Mittiga, S. Hsieh, C. Zu, B. Kobrin, F. Machado, P. Bhattacharyya, N. Z. Rui, A. Jarmola, S. Choi, D. Budker, and N. Y. Yao

Imaging the local charge environment of nitrogen-vacancy centers in diamond

T. Mittiga,[1, *] S. Hsieh,[1, 2, *] C. Zu,[1, *] B. Kobrin,[1, 2] F. Machado,[1] P. Bhattacharyya,[1, 2]
N. Z. Rui,[1] A. Jarmola,[1, 3] S. Choi,[1] D. Budker,[4, 1] and N. Y. Yao[1, 2]

[1]*Department of Physics, University of California, Berkeley, CA 94720, USA*
[2]*Materials Science Division, Lawrence Berkeley National Laboratory, Berkeley, CA 94720, USA*
[3]*U.S. Army Research Laboratory, Adelphi, MD 20783, USA*
[4]*Helmholtz Institut, Johannes Gutenberg-Universität Mainz, 55099 Mainz, Germany*

Characterizing the local *internal* environment surrounding solid-state spin defects is crucial to harnessing them as nanoscale sensors of *external* fields. This is especially germane to the case of defect ensembles which can exhibit a complex interplay between interactions, internal fields and lattice strain. Working with the nitrogen-vacancy (NV) center in diamond, we demonstrate that local electric fields dominate the magnetic resonance behavior of NV ensembles at low magnetic field. We introduce a simple microscopic model that quantitatively captures the observed spectra for samples with NV concentrations spanning over two orders of magnitude. Motivated by this understanding, we propose and implement a novel method for the nanoscale localization of individual charges within the diamond lattice; our approach relies upon the fact that the charge induces an NV dark state which depends on the electric field orientation.

A tremendous amount of recent effort has focused on the creation and control of nanoscale defects in the solid-state [1, 2]. The spectral properties of these defects often depend sensitively on their environment. On the one hand, this sensitivity naturally suggests their use as nanoscale quantum sensors of *external* signals. On the other hand, accurately quantifying these signals requires the careful characterization of *internal* local fields. Here, we focus on a particular defect, the negatively charged nitrogen-vacancy (NV) color center in diamond [2, 3]. The electronic spin associated with the NV center is sensitive to a broad range of external signals, from magnetic and electric fields to pressure, temperature and gyroscopic precession [4–13]. Isolated single NVs have been used to explore phenomena in biology [2, 14, 15], materials science [16–20], and fundamental physics [21–23].

More recently, many-body correlations have emerged as a powerful resource for enhancing the sensitivity of interacting spin ensembles [24–28]. To this end, a number of studies have explored and leveraged the properties of high-density NV systems [7, 29–40]. The local environment in such systems is substantially more complex than that of isolated NVs; this arises from a competition between multiple effects, including: lattice strain, paramagnetic impurities, charge dynamics, and NV-NV dipolar interactions. While the presence of an applied external magnetic field can suppress some of these effects, it significantly limits the scope of sensing applications such as zero-field nuclear magnetic resonance spectroscopy [41, 42]. Thus, characterizing and understanding the spectral properties of NV ensembles at zero field is crucial to utilizing these systems as quantum sensors.

In this Letter, we present three main results. First, we demonstrate that the characteristic splitting of the NV's magnetic resonance spectrum (Fig. 1a), observed in ensemble NV experiments [9, 14, 43–59], originates from its local electric environment [60]; this contrasts
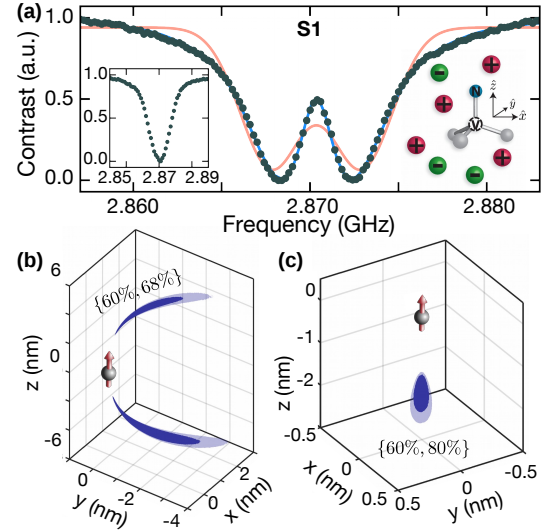

FIG. 1. Typical optically-detected magnetic resonance (ODMR) spectrum of an electron-irradiated and annealed Type-Ib diamond sample (S1) at zero magnetic field. The spectrum exhibits heavy tails which cannot be reproduced by either a double Lorentzian or Gaussian (orange fit) profile. The blue theory curve is obtained via our microscopic charge model. (Left inset) A typical zero-field spectrum for a single NV center shows only a single resonance. (Right inset) Schematic depicting an equal density of positive (e.g. N^+) and negative (e.g. NV) charges, which together, create a random local electric field at each NV center's position. (b) Nanoscale localization ($\sim$5 nm) of a single positive charge via dark-state spectroscopy of an isolated NV center. The shaded regions indicate the probable location of the charge with darker indicating a higher likelihood. Percentages shown correspond to the confidence intervals of the dark/light region, respectively. (c) Analogous localization of a more proximal charge defect ($\sim$2 nm) for a different NV center.

with the conventional picture that strain dominates the zero-field properties of these systems. Second, we in-
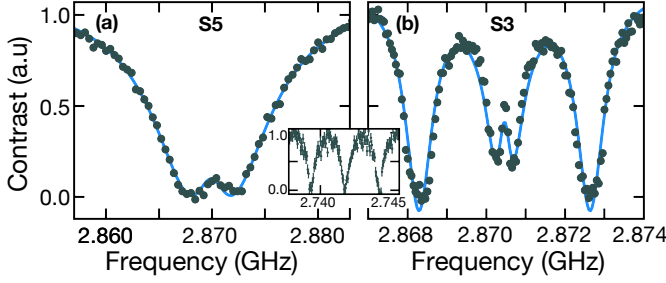
FIG. 2. ODMR spectra at zero magnetic field for (a) a Type-Ib untreated diamond sample (S5) and (b) a Type-IIa electron-irradiated and annealed sample (S3). The spectra portray the two qualitative regimes one expects based upon the average electric field strength as shown schematically in the right panel of Fig. 3d. The blue theory curve is obtained via our microscopic charge model. (inset) The spectrum for S3 at a magnetic field ≈ 45 G exhibits three identical hyperfine resonances.
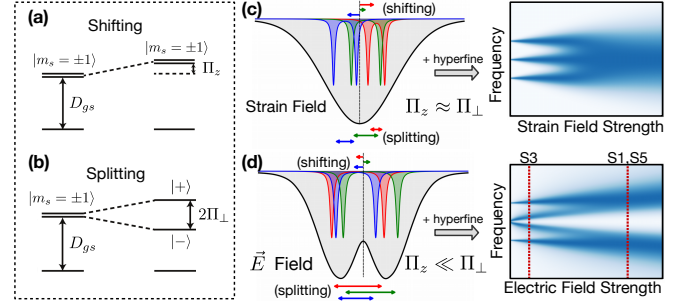

FIG. 3. Both strain and electric fields lead to (a) shifting Π_z and (b) splitting $2\Pi_\perp$ of the $|m_s = \pm 1\rangle$ manifold. (c) When averaged over an ensemble of NV centers, random local strain fields lead to a single broad spectral feature (at large strain). (d) In contrast, random local electric fields lead to two distinct spectral regimes: at small electric fields, the center hyperfine resonance splits, leading to a total of four resolvable features (S3); at large electric field, one obtains the characteristic split resonance seen in typical high density NV ensembles (S1, S5).

troduce a charge-based model (Fig. 1a, right inset) that quantitatively reproduces the observed ODMR spectra for samples spanning two orders of magnitude in NV density. Third, our model suggests the ability to directly *image* the position of individual charges inside the diamond lattice. To this end, we propose and implement a novel method that localizes such charges to nanometer-size volumes (Fig. 1b,c). The essence of our approach is to leverage the interplay between the polarization of the applied microwave field and the orientation of the local electric field.

Magnetic spectra of NV ensembles—The NV center has a spin triplet ground state ($|m_s = \pm 1, 0\rangle$), which can be initialized and read out via optical excitation and coherently manipulated using microwave fields [61]. In the absence of any external perturbations, the $|m_s = \pm 1\rangle$ states are degenerate and separated from $|m_s = 0\rangle$ by $D_{\mathrm{gs}} = (2\pi) \times 2.87$ GHz (Fig. 3a).

This leads to the usual expectation of a single resonance peak at D_{gs}, consistent with experimental observations of isolated NVs (Fig. 1a, inset). However, for high-density NV ensembles, one observes a qualitatively distinct spectrum, consisting of a pair of resonances centered at D_{gs} (Fig. 1a, sample S1). This spectrum poses a number of puzzles: First, the line-shape of each resonance is asymmetric and cannot be captured by either a Gaussian or Lorentzian profile. Second, the central feature between the resonances is sharper than the inhomogenous linewidth. Third, despite the presence of a strong *splitting*, there exists almost no *shift* of the NV's overall spectrum.

These generic features are present in diamond samples with NV and P1 (nitrogen impurity) densities spanning over two orders of magnitude. Fig. 2 demonstrates this ubiquity. In particular, it depicts the spectrum for two other samples: one with a significantly lower NV

concentration (Fig. 2a, sample S5) and a second with significantly lower concentrations for both NVs and P1s (Fig. 2b, sample S3). In this latter case, the P1 density is low enough that the hyperfine interaction between the NV's electronic spin and its host ^{14}N nuclear spin can be resolved. Normally, this hyperfine splitting would simply result in three identical resonances split from one another by $A_{zz} = (2\pi) \times 2.16$ MHz [62] (Fig. 2, inset). However, as shown in Fig. 2b, one finds that the central hyperfine resonance is split in direct analogy to the prior spectra.

The most distinct of the aforementioned features – a split central resonance – has typically been attributed to the presence of lattice strain [9, 44–59]. Such strain can indeed lead to a coupling between the $|m_s = \pm 1\rangle$ states, and thus split their energy levels. However, a more careful analysis reveals an important inconsistency. In particular, given the measured strain susceptibility parameters [44], for each individual NV, any strain-induced splitting should be accompanied by a comparable shift of the overall spectrum (Fig. 3). Ensemble averaging then naturally leads to a spectrum that exhibits *only* a single broadened resonance (Fig. 3c).

Microscopic charge model—In contrast, we demonstrate that all of the observed features can be quantitatively explained via a microscopic model based upon randomly positioned charges inside the diamond lattice. The physical intuition underlying this model is simple: each (negatively charged) NV center plays the role of an electron acceptor, and charge neutrality implies that there must be a corresponding positively charged electron donor (typically thought to be N^+, a positively charged P1 center).

Such charges produce an electric field that also (like strain) couples the $|m_s = \pm 1\rangle$ states, leading to the splitting of the resulting eigenstates. Crucially, however,

Sample	ρ_c (ppm)	ρ_{NV} (ppm)	ρ_s (ppm)	Γ (MHz)
Ib treated (S1)	1.35(5)	1-10	70(5)	1.16(2)
Ib treated (S2)	1.7(1)	1-10	100(5)	0.78(3)
IIa treated (S3)	0.06(2)	0.01-0.1	12(3)	0.26(2)
Ib untreated (S4)	3.6(4)	0.001-0.01	90(20)	1.0(1)
Ib untreated (S5)	0.9(2)	0.001-0.01	130(30)	3.3(1)
IIa untreated (S6)	0.05(1)	0.001-0.01	16(2)	0.08(3)

TABLE I. Summary of the measured and extracted parameters for each diamond sample. ρ_c and Γ are directly extracted from our microscopic model, while ρ_s is independently measured at high magnetic fields and ρ_{NV} is estimated from fluorescence counts [67].
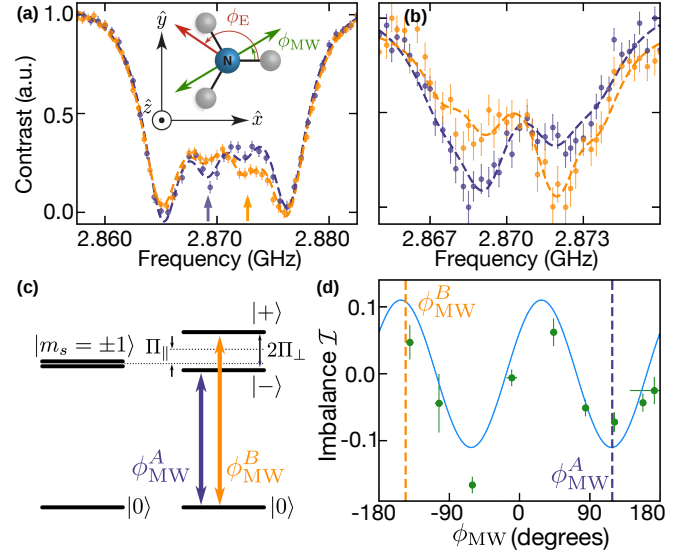

FIG. 4. Charge localization via dark-state spectroscopy. (a) Single NV ODMR spectra (untreated Type-Ib diamond) for two different microwave polarizations, ϕ_{MW}, depicting the reversal of the split-peak imbalance. The data correspond to the localized charge shown in Fig. 1b. (inset) Top view through the NV-axis ($\hat{z}$), where ϕ_E and ϕ_{MW} are defined with respect to $\hat{x}$ (along a carbon-vacancy bond). (b) Analogous split-peak imbalance data corresponding to the localized charge shown in Fig. 1c. (c) By changing the microwave polarization, ϕ_{MW}, one can directly control the coupling strength between the $|0\rangle$ and $|\pm\rangle$ states. (d) Measuring the change in the imbalance as a function of ϕ_{MW} allows one to extract the orientation of the electric field. Dashed lines indicate the polarizations plotted in (a).

the NV's susceptibility to transverse electric fields (which cause splitting) is $\sim$50 times larger than its susceptibility to axial electric fields (which cause shifting) [63, 64]. This implies that even upon ensemble averaging, the electric-field-induced splitting remains prominent (Fig. 3d).

Qualitative picture in hand, let us now introduce the details of our microscopic model. In particular, we consider each NV to be surrounded by an equal density, ρ_c, of positive and negative charges [65]. These charges generate a local electric field at the position of the NV center and couple to its spin via the Hamiltonian:

$$H = (D_{gs} + \Pi_z) S_z^2 + (\delta B_z + A_{zz} I_z) S_z + \Pi_x (S_y^2 - S_x^2) + \Pi_y (S_x S_y + S_y S_x). \quad (1)$$

Here, $\hat{z}$ is the NV-axis, $\hat{x}$ is defined such that one of the carbon-vacancy bonds lies in the x-z plane (Fig. 1a, right inset), $\vec{S}$ are the electronic spin-1 operators of the NV, $\vec{I}$ are the nuclear spin-1 operators of the host ^{14}N [66], and δB_z represents a random local magnetic field (for example, generated by nearby paramagnetic impurities). Note that we absorb the gyromagnetic ratio into δB_z. The two terms $\Pi_{\{x,y\}} = d_\perp E_{\{x,y\}}$ and $\Pi_z = d_\parallel E_z$ characterize the NV's coupling to the electric field, $\vec{E}$, with susceptibilities $\{d_\parallel, d_\perp\} = \{0.35, 17\}$ Hz cm/V [63].

In order to obtain the spectra for a single NV, we sample $\vec{E}$ and δB_z from their random distributions and then diagonalize the Hamiltonian. Moreover, to account for the natural linewidth of each resonance, we include an additional Lorentzian broadening with full-width-half-maximum, Γ [67]. Averaging over this procedure yields the ensemble spectrum. The distribution of $\vec{E}$ is determined by the random positioning of the aforementioned charges. The distribution of δB_z is determined by the local magnetic environment, which depends sensitively on the concentration of spin defects (Table I).

In samples S1 and S5 (Type-Ib diamond), δB_z is dominated by the dipolar interaction with a high-density P1 spin bath, whose concentration, ρ_s, is independently characterized [67]. Meanwhile, in sample S3 (Type-IIa diamond), the P1 density is over two orders of magni-

tude smaller, leading to a δB_z that is dominated by interactions with ^{13}C nuclei (with a natural abundance of 1.1%); despite this difference in microscopic origin, one can also characterize the effect of this nuclear spin bath using an effective density, ρ_s [67]. For each sample, using this independently characterized ρ_s, we then fit the experimental spectrum by varying ρ_c and Γ. We find excellent agreement for all three samples (Fig. 1, 2) despite their vastly different defect concentrations (Table I).

A few remarks are in order. First, the presence of local electric fields suppresses the effect of magnetic noise when $\delta B_z \ll \Pi_\perp = \sqrt{\Pi_x^2 + \Pi_y^2}$. This is precisely the origin for both the sharpness of the inner central feature seen in Fig. 1a, as well as the narrowness of the inner hyperfine resonances seen in Fig. 2b. Second, in samples where the electric field dominates, the long-range, power-law nature of the electric field leads to a particularly heavy tailed spectrum [67]. Third, the extracted charge density, ρ_c, is consistent with the estimated NV density, ρ_{NV}, for all "treated" (electron-irradiated and annealed) samples (S1-S3). This agrees with our previous physical intuition: NVs behave as electron acceptors while P1s behave as electron donors. Interestingly, this

simple picture does not directly translate to "untreated" samples (S4-S6) where the observed charge density is significantly larger than ρ_{NV} (Table I); one possible explanation is that such samples harbor a higher density of non-NV charged defects (e.g. vacancy complexes [68]).

Nanoscale imaging of a single charge—Our microscopic model suggests that in samples where one can resolve single NV centers, it should be possible to directly probe the *local* charge environment. However, one expects a key difference in contrast to ensemble measurements: for a single NV, the electric field has a definite orientation with respect to the NV axes (Fig. 4a diagram).

Crucially, this orientation (namely, the angle, ϕ_E, in the NV's transverse plane) dictates the way in which the electric field mixes the original $|m_s = \pm 1\rangle$ states into bright and dark states:

$$|\pm\rangle = \frac{1}{\sqrt{2}} \left(|m_s = +1\rangle \mp e^{-i\phi_E}|m_s = -1\rangle \right). \quad (2)$$

Applying a linearly polarized microwave field will then drive transitions between the $|m_s = 0\rangle$ state and the $|\pm\rangle$ states. However, the relative strength of the two transitions depends on both ϕ_E and the polarization of the microwave field, ϕ_{MW} (Fig. 4c). Thus, one generally expects the measured amplitudes of the corresponding resonances to be different. These expectations are indeed borne out by the data (Fig. 4a,b) [69]. We note that this observed imbalance in the inner hyperfine resonances for a *single* NV is naturally averaged out in an ensemble measurement.

Our detailed understanding of this spectroscopy for a single NV suggests a novel method to extract the full vector electric field and to localize the position of the corresponding charge. In particular, by measuring the imbalance as a function of ϕ_{MW}, one can extract the electric field orientation, ϕ_E. More specifically, we define the imbalance, $\mathcal{I} \equiv \frac{A_+ - A_-}{A_+ + A_-}$, where $A_\pm$ are the amplitudes of the $|m_s = 0\rangle \leftrightarrow |\pm\rangle$ resonances and derive [67]:

$$\mathcal{I} \sim -\cos(2\phi_{MW} + \phi_E). \quad (3)$$

Thus, $\phi_E = 124(5)°$ can be extracted as the phase offset in Fig. 4d. In combination with the observed splitting and shifting of the inner resonances, $\Pi_z = 30(50)$ kHz, $\Pi_\perp = 650(10)$ kHz, one can fully reconstruct the local electric field vector [67, 70]. We do not observe any changes to this field over the course of the experiment (months) and find that it varies for different NV centers. This suggests that it originates from a stationary local charge environment. Moreover, charge neutrality and a low defect density suggest that the electric field is generated by a single positive charge, which we can then localize to within a nanoscale volume (Fig. 1b,c).

Summary and outlook—While it is abundantly asserted in the literature that the zero-field spectral features of NV ensembles owe to lattice strain, here, we demonstrate that such spectra are in fact dominated by the effect of local electric fields. Using a microscopic charge model, we quantitatively capture the magnetic resonance spectra of NV ensembles for defect concentrations spanning two orders of magnitude. Moreover, we introduce a method to image the spatial location of individual charges near a single NV center with nanoscale precision.

These results open the door to a number of intriguing future directions. First, although we observe charge densities that are consistent with the NV density in all treated samples (and thus consistent with a picture for charge neutrality), we find a deviation from this understanding for untreated samples which exhibit an anomalously large charge density. Further study is necessary to reveal the precise nature of these additional charges [60]. Second, our results provide an improved understanding of NV ensembles at low magnetic fields; this is of particular relevance to the sensing of electric fields, lattice strain and gyroscopic precession, as well as to studies of magnetically sensitive quantum materials. Third, the charge-induced suppression of δB_z suggests the possibility of enhancing the NV's resilience to magnetic noise. Finally, understanding the local charge environment of single NV centers could provide insights into the optical spectral diffusion observed at low temperatures [71, 72].

---

* These authors contributed equally to this work

[1] I. Aharonovich, D. Englund, and M. Toth, Nature Photonics **10**, 631 (2016).

[2] R. Schirhagl, K. Chang, M. Loretz, and C. L. Degen, Annual Review of Physical Chemistry **65**, 83 (2014), pMID: 24274702, https://doi.org/10.1146/annurev-physchem-040513-103659.

[3] M. W. Doherty, N. B. Manson, P. Delaney, F. Jelezko, J. Wrachtrup, and L. C. Hollenberg, Physics Reports **528**, 1 (2013).

[4] J. Maze, P. Stanwix, J. Hodges, S. Hong, J. Taylor, P. Cappellaro, L. Jiang, M. G. Dutt, E. Togan, A. Zibrov, *et al.*, Nature **455**, 644 (2008).

[5] H. Mamin, M. Kim, M. Sherwood, C. Rettner, K. Ohno, D. Awschalom, and D. Rugar, Science **339**, 557 (2013).

[6] D. Toyli, D. Christle, A. Alkauskas, B. Buckley, C. Van de Walle, and D. Awschalom, Physical Review X **2**, 031001 (2012).

[7] V. M. Acosta, E. Bauch, A. Jarmola, L. J. Zipp, M. P. Ledbetter, and D. Budker, Applied Physics Letters **97**, 174104 (2010).

[8] R. Epstein, F. Mendoza, Y. Kato, and D. Awschalom, Nature physics **1**, 94 (2005).

[9] F. Dolde, H. Fedder, M. W. Doherty, T. Nöbauer, F. Rempp, G. Balasubramanian, T. Wolf, F. Reinhard, L. C. L. Hollenberg, F. Jelezko, and J. Wrachtrup, Nature Physics **7**, 459 (2011).

[10] F. Dolde, M. W. Doherty, J. Michl, I. Jakobi, B. Naydenov, S. Pezzagna, J. Meijer, P. Neumann, F. Jelezko, N. B. Manson, and J. Wrachtrup, Physical Review Letters **112**, 097603 (2014).

[11] M. W. Doherty, V. V. Struzhkin, D. A. Simpson, L. P. McGuinness, Y. Meng, A. Stacey, T. J. Karle, R. J. Hemley, N. B. Manson, L. C. Hollenberg, *et al.*, Physical review letters **112**, 047601 (2014).

[12] M. P. Ledbetter, K. Jensen, R. Fischer, A. Jarmola, and D. Budker, Physical Review A **86**, 052116 (2012).

[13] A. Ajoy and P. Cappellaro, Physical Review A **86**, 062104 (2012).

[14] G. Kucsko, P. C. Maurer, N. Y. Yao, M. Kubo, H. J. Noh, P. K. Lo, H. Park, and M. D. Lukin, Nature **500**, 54 (2013).

[15] L. P. McGuinness, Y. Yan, A. Stacey, D. A. Simpson, L. T. Hall, D. Maclaurin, S. Prawer, P. Mulvaney, J. Wrachtrup, F. Caruso, R. E. Scholten, and L. C. L. Hollenberg, Nature Nanotechnology **6**, 358 EP (2011).

[16] A. Laraoui, H. Aycock-Rizzo, Y. Gao, X. Lu, E. Riedo, and C. A. Meriles, Nature Communications **6**, 8954 (2015).

[17] M. Pelliccione, A. Jenkins, P. Ovartchaiyapong, C. Reetz, E. Emmanouilidou, N. Ni, and A. C. B. Jayich, Nature nanotechnology **11**, 700 (2016).

[18] C. Du, T. Van der Sar, T. X. Zhou, P. Upadhyaya, F. Casola, H. Zhang, M. C. Onbasli, C. A. Ross, R. L. Walsworth, Y. Tserkovnyak, *et al.*, Science **357**, 195 (2017).

[19] Y. Dovzhenko, F. Casola, S. Schlotter, T. X. Zhou, F. Büttner, R. L. Walsworth, G. S. Beach, and A. Yacoby, arXiv preprint arXiv:1611.00673 (2016).

[20] I. Gross, W. Akhtar, V. Garcia, L. Martínez, S. Chouaieb, K. Garcia, C. Carrétéro, A. Barthélémy, P. Appel, P. Maletinsky, *et al.*, Nature **549**, 252 (2017).

[21] G. Waldherr, P. Neumann, S. Huelga, F. Jelezko, and J. Wrachtrup, Physical Review Letters **107**, 090401 (2011).

[22] H. Bernien, B. Hensen, W. Pfaff, G. Koolstra, M. Blok, L. Robledo, T. Taminiau, M. Markham, D. Twitchen, L. Childress, *et al.*, Nature **497**, 86 (2013).

[23] B. Hensen, H. Bernien, A. E. Dréau, A. Reiserer, N. Kalb, M. S. Blok, J. Ruitenberg, R. F. L. Vermeulen, R. N. Schouten, C. Abellán, W. Amaya, V. Pruneri, M. W. Mitchell, M. Markham, D. J. Twitchen, D. Elkouss, S. Wehner, T. H. Taminiau, and R. Hanson, Nature **526**, 682 (2015).

[24] W. Wasilewski, K. Jensen, H. Krauter, J. J. Renema, M. Balabas, and E. S. Polzik, Physical Review Letters **104**, 133601 (2010).

[25] S. Simmons, J. A. Jones, S. D. Karlen, A. Ardavan, and J. J. Morton, Physical Review A **82**, 022330 (2010).

[26] J. A. Jones, S. D. Karlen, J. Fitzsimons, A. Ardavan, S. C. Benjamin, G. A. D. Briggs, and J. J. Morton, Science **324**, 1166 (2009).

[27] P. Cappellaro and M. D. Lukin, Physical Review A **80**, 032311 (2009).

[28] S. Choi, N. Y. Yao, and M. D. Lukin, ArXiv e-prints (2018), arXiv:1801.00042 [quant-ph].

[29] V. M. Acosta, E. Bauch, M. P. Ledbetter, C. Santori, K. M. C. Fu, P. E. Barclay, R. G. Beausoleil, H. Linget, J. F. Roch, F. Treussart, S. Chemerisov, W. Gawlik, and D. Budker, Physical Review B **80**, 115202 (2009).

[30] S. Steinert, F. Dolde, P. Neumann, A. Aird, B. Naydenov, G. Balasubramanian, F. Jelezko, and J. Wrachtrup, Review of Scientific Instruments **81**, 043705 (2010).

[31] B. Maertz, A. Wijnheijmer, G. Fuchs, M. Nowakowski, and D. Awschalom, Applied Physics Letters **96**, 092504 (2010).

[32] P. L. Stanwix, L. M. Pham, J. R. Maze, D. Le Sage, T. K. Yeung, P. Cappellaro, P. R. Hemmer, A. Yacoby, M. D. Lukin, and R. L. Walsworth, Physical Review B **82**, 201201 (2010).

[33] L. M. Pham, D. Le Sage, P. L. Stanwix, T. K. Yeung, D. Glenn, A. Trifonov, P. Cappellaro, P. R. Hemmer, M. D. Lukin, H. Park, A. Yacoby, and R. L. Walsworth, New Journal of Physics **13**, 045021 (2011).

[34] A. Jarmola, V. M. Acosta, K. Jensen, S. Chemerisov, and D. Budker, Physical Review Letters **108**, 197601 (2012).

[35] N. Bar-Gill, L. M. Pham, A. Jarmola, D. Budker, and R. L. Walsworth, Nature Communications **4**, 1743 (2013).

[36] D. Le Sage, K. Arai, D. Glenn, S. DeVience, L. Pham, L. Rahn-Lee, M. Lukin, A. Yacoby, A. Komeili, and R. Walsworth, Nature **496**, 486 (2013).

[37] A. Jarmola, A. Berzins, J. Smits, K. Smits, J. Prikulis, F. Gahbauer, R. Ferber, D. Erts, M. Auzinsh, and D. Budker, Applied Physics Letters **107**, 242403 (2015).

[38] T. Wolf, P. Neumann, K. Nakamura, H. Sumiya, T. Ohshima, J. Isoya, and J. Wrachtrup, Physical Review X **5**, 041001 (2015).

[39] J. F. Barry, M. J. Turner, J. M. Schloss, D. R. Glenn, Y. Song, M. D. Lukin, H. Park, and R. L. Walsworth, Proceedings of the National Academy of Sciences **113**, 14133 (2016).

[40] D. R. Glenn, R. R. Fu, P. Kehayias, D. Le Sage, E. A. Lima, B. P. Weiss, and R. L. Walsworth, Geochemistry, Geophysics, Geosystems **18**, 3254 (2017).

[41] D. Weitekamp, A. Bielecki, D. Zax, K. Zilm, and A. Pines, Physical review letters **50**, 1807 (1983).

[42] A. M. Thayer and A. Pines, Accounts of Chemical Research **20**, 47 (2002).

[43] A. Gruber, A. Dräbenstedt, C. Tietz, L. Fleury, J. Wrachtrup, and C. von Borczyskowski, Science **276**, 2012 (1997).

[44] M. S. J. Barson, P. Peddibhotla, P. Ovartchaiyapong, K. Ganesan, R. L. Taylor, M. Gebert, Z. Mielens, B. Koslowski, D. A. Simpson, L. P. McGuinness, J. McCallum, S. Prawer, S. Onoda, T. Ohshima, A. C. B. Jayich, F. Jelezko, N. B. Manson, and M. W. Doherty,

Nano Letters **17**, 1496 (2017).

[45] R. Igarashi, Y. Yoshinari, H. Yokota, T. Sugi, F. Sugihara, K. Ikeda, H. Sumiya, S. Tsuji, I. Mori, H. Tochio, Y. Harada, and M. Shirakawa, Nano Letters **12**, 5726 (2012).

[46] J. Forneris, S. Ditalia Tchernij, P. Traina, E. Moreva, N. Skukan, M. Jakšić, V. Grilj, L. Croin, G. Amato, I. P. Degiovanni, B. Naydenov, F. Jelezko, M. Genovese, and P. Olivero, ArXiv e-prints (2017), arXiv:1706.07935 [cond-mat.mtrl-sci].

[47] X. Zhu, Y. Matsuzaki, R. Amsüss, K. Kakuyanagi, T. Shimo-Oka, N. Mizuochi, K. Nemoto, K. Semba, W. J. Munro, and S. Saito, Nature Communications **5**, 3424 (2014).

[48] M. Simanovskaia, K. Jensen, A. Jarmola, K. Aulenbacher, N. Manson, and D. Budker, Phys. Rev. B **87**, 224106 (2013).

[49] V. M. Acosta, E. Bauch, M. P. Ledbetter, A. Waxman, L.-S. Bouchard, and D. Budker, Phys. Rev. Lett. **104**, 070801 (2010).

[50] Y. Kubo, F. R. Ong, P. Bertet, D. Vion, V. Jacques, D. Zheng, A. Dréau, J. F. Roch, A. Auffèves, F. Jelezko, J. Wrachtrup, M. F. Barthe, P. Bergonzo, and D. Esteve, Physical Review Letters **105**, 140502 (2010).

[51] N. D. Lai, D. Zheng, F. Jelezko, F. Treussart, and J.-F. Roch, Applied Physics Letters **95**, 133101 (2009), https://doi.org/10.1063/1.3238467.

[52] E. Bourgeois, A. Jarmola, P. Siyushev, M. Gulka, J. Hruby, F. Jelezko, D. Budker, and M. Nesladek, Nature Communications **6**, 8577 (2015).

[53] L. Rondin, J.-P. Tetienne, T. Hingant, J. F. Roch, P. Maletinsky, and V. Jacques, Reports on Progress in Physics **77**, 056503 (2014).

[54] P. Jamonneau, M. Lesik, J. P. Tetienne, I. Alvizu, L. Mayer, A. Dréau, S. Kosen, J.-F. Roch, S. Pezzagna, J. Meijer, T. Teraji, Y. Kubo, P. Bertet, J. R. Maze, and V. Jacques, Phys. Rev. B **93**, 024305 (2016).

[55] M. Simanovskaia, K. Jensen, A. Jarmola, K. Aulenbacher, N. Manson, and D. Budker, Phys. Rev. B **87**, 224106 (2013).

[56] Y. Matsuzaki, H. Morishita, T. Shimooka, T. Tashima, K. Kakuyanagi, K. Semba, W. J. Munro, H. Yamaguchi, N. Mizuochi, and S. Saito, Journal of Physics: Condensed Matter **28**, 275302 (2016).

[57] E. H. Chen, H. A. Clevenson, K. A. Johnson, L. M. Pham, D. R. Englund, P. R. Hemmer, and D. A. Braje, Phys. Rev. A **95**, 053417 (2017).

[58] A. O. Levchenko, V. V. Vasil'ev, S. A. Zibrov, A. S. Zibrov, A. V. Sivak, and I. V. Fedotov, Applied Physics Letters **106**, 102402 (2015), https://doi.org/10.1063/1.4913428.

[59] L. G. Steele, M. Lawson, M. Onyszczak, B. T. Bush, Z. Mei, A. P. Dioguardi, J. King, A. Parker, A. Pines, S. T. Weir, W. Evans, K. Visbeck, Y. K. Vohra, and N. J. Curro, Applied Physics Letters **111**, 221903 (2017).

[60] N. B. Manson, M. Hedges, J. Barson, R. Ahlefeldt, M. W. Doherty, M. J. Sellars, H. Abe, T. Ohshima, *et al.*, arXiv preprint arXiv:1807.08889 (2018).

[61] J. R. Maze, A. Gali, E. Togan, Y. Chu, A. Trifonov, E. Kaxiras, and M. D. Lukin, New Journal of Physics **13**, 025025 (2011).

[62] B. Smeltzer, L. Childress, and A. Gali, New Journal of Physics **13**, 025021 (2011).

[63] E. V. Oort and M. Glasbeek, Chemical Physics Letters

168, 529 (1990).

[64] Kobrin et al., in preparation (2018).

[65] We assume that the charges are independently positioned in three dimensions.

[66] We note that the the hyperfine interaction in the Hamiltonian is obtained under the secular approximation.

[67] See Supplementary Material for additional details.

[68] G. Davies, Nature **269**, 498 (1977).

[69] We measure the ODMR spectra of 68 single NV centers in an untreated Type-Ib sample, and find four that exhibit a significant electric-field-induced splitting with amplitude difference at zero magnetic field [67].

[70] S. Whitehead and W. Hackett, Proceedings of the Physical Society **51**, 173 (1939).

[71] Y. Chu, N. P. de Leon, B. J. Shields, B. Hausmann, R. Evans, E. Togan, M. J. Burek, M. Markham, A. Stacey, A. S. Zibrov, A. Yacoby, D. J. Twitchen, M. Loncar, H. Park, P. Maletinsky, and M. D. Lukin, Nano Letters **14**, 1982 (2014).

[72] F. Jelezko, I. Popa, A. Gruber, C. Tietz, J. Wrachtrup, A. Nizovtsev, and S. Kilin, Applied Physics Letters **81**, 2160 (2002).